

0EFZS--4555

Oktober 1990

AT9000218



Österreichisches Forschungszentrum

Seibersdorf

Calculation of the Source Term for a  
 $S_1B$ -Sequence at a VVER-1000 Type Reactor  
Part 1

Gert Sdouz

CALCULATION OF THE SOURCE TERM FOR A  $S_1$ B-SEQUENCE  
AT A VVER-1000 TYPE REACTOR  
Part 1

Gert Sdouz

Arbeitsbericht

Österreichisches  
Forschungszentrum Seibersdorf  
Ges.m.b.H.  
ENGINEERING  
ENERGIE- UND ANLAGENTECHNIK  
A-2444 Seibersdorf

CALCULATION OF THE SOURCE TERM  
FOR A S<sub>1</sub>B-SEQUENCE AT A VVER-1000 TYPE REACTOR

ABSTRACT

The behaviour of the source term in a VVER-1000 type reactor is calculated using the "Source Term Code Package" (STCP). The input data are based on the russian plant Zaporozhye-5. The selected accident sequence is a small break LOCA in the hot leg followed by loss of offsite and onsite electric power (S<sub>1</sub>B-sequence). According to the course of the calculation the results are presented and analyzed for each program. Except for the noble gases all release fractions are lower than 10<sup>-4</sup>.

BERECHNUNG DES QUELLTERMS FÜR EINEN  
S<sub>1</sub>B-STÖRFALL BEI EINEM REAKTOR VOM TYP VVER-1000

KURZFASSUNG

Mit Hilfe des "Source Term Code Package" (STCP) wird das Verhalten des Quellterms in einem VVER-1000 Reaktor berechnet. Die Eingabedaten beruhen auf den Spezifikationen des russischen Kraftwerks Zaporozhye-5. Der Störfall wurde durch einen Kühlmittelverlust mit kleinem Leck im heißen Ast ausgelöst, dem ein Ausfall der Stromversorgung folgte (S<sub>1</sub>B-Sequenz). Gemäß dem Rechenablauf werden die Ergebnisse Programm für Programm beschrieben und analysiert. Außer bei den Edelgasen betragen alle Freisetzungsraten weniger als 10<sup>-4</sup>.

INIS-FACHBEREICH: E 32.00

INIS-DESKRIPTOREN: Reactor Accidents/Meltdown/WWER Type Reactors/Fission Product Release

ACKNOWLEDGEMENT

On the occasion of the increased scientific cooperation between east and west this work is dedicated to all international friends who contributed to the progress of source term studies. Special appreciation is extended to M.W. Jankowski (IAEA, Division of Nuclear Safety) for organizing the Regional Programme on severe accident analysis of the VVER-type reactors. During the sessions of the various workshops contacts could be established between colleagues from Bulgaria, Czechoslovakia, Germany, Hungary, Poland, USSR and Austria. The author is grateful to Dr. V. Asmolov for hosting two of the workshops in Kurchatov Institute in Moscow. Many fruitful discussions with Dr.-Ing. G. Preußer (KWU) and the colleagues of the OECD Task Groups FPC and SAC inspired this work.

Finally the author would like to thank M. Pachole for producing the huge amount of plots and M. Witt for her extremely able converting the handwriting into a readable typed version.

Without the financial support of the Austrian BKA represented by DI G. Wagner this work would not have been possible.

CONTENTS

	page
1. INTRODUCTION .....	1
2. S <sub>1</sub> B-SEQUENCE .....	3
3. INPUT-DATA .....	5
3.1 MARCH3 .....	5
3.2 TRAPT-MELT3.....	11
3.3 VANESA .....	15
3.4 NAUA AND THCCA .....	15
4. RESULTS .....	19
4.1 MARCH3 - Thermalhydraulics .....	19
4.2 TRAP-MELT3 - Fission Product Transport in Primary System.....	31
4.3 VANESA - Fission Product Release during Debris-Concrete Interaction.....	36
4.4 NAUA - Fission Product Transport in Containment..	40
5. DISCUSSION .....	45
6. REFERENCES .....	48
7. LIST OF FIGURES .....	50

Note: This report is published in 2 parts.  
Part 1 contains the text and the tables.  
The figures are published in Part 2.

## 1. INTRODUCTION

In the development of the nuclear industry highest importance was attached to safety and every effort was made to protect the operators and the public. Since 1950 the effects of postulated accidents at nuclear power plants are investigated. During the last decade a lot of work was performed to investigate severe accidents.

In these studies the central term is "risk". Risk is defined as the combination of the frequency of an event and the consequences of this event. The size of the consequences depends on the amount of released radioactivity - the so-called "source term", on the transport to the population and on the different biological effects. To estimate the risk of a plant it is necessary to select accident scenarios. The first step of a calculation is the determination of the source term. The result of a source term calculation for a specific accident sequence is the fraction of core inventory which is released to the environment.

In the USA several important reports on source term behaviour were published: NUREG-0772 [1], NUREG-0771 [2] and NUREG-0773 [3]. Based on the results of these studies and on the growing data base a new study was sponsored by NRC. This study was performed by Battelle Columbus and published as NUREG-0956 [4] in 1986. For this study several codes were developed to simulate severe accidents. Finally the codes were combined into a system (Fig. 1) and published as "Source Term Code Package" (STCP) [5]. At last a new risk-study was performed using the STCP. The results are published recently in NUREG-1150 [6].

For most of the western reactor types risk studies were performed. Austria however is surrounded by a number of VVER-type reactors for which no risk studies or source term studies exist. Therefore we decided to apply STCP on VVER-type reactors. Our goal is to do source term calculations for several different accident sequences and detect possibilities to improve the safety of these reactors.

The STCP was obtained from the developer Battelle Columbus. We decided to use the CDC-version of the code because the complexity of the calculation demands high computation speed. In a first step the STCP was implemented on a CYBER 180/860 [7]. This work was completed with a successful calculation of the sample problem.

For the first calculations the VVER-1000 type reactor was selected. In the next years about 50 units of VVER-1000 are planned in eastern europe. This number stresses the importance of a source term study for these reactors.

As first accident sequence a transient initiated event with failure of all makeup to the primary and secondary systems as well as the failure of all active containment safety features (TMLB') was selected. The results showed a fission product behaviour quite similar to that in western-type reactors [8].

The next steps were the improvement of basic input data (chapter 3) and the calculation for a different accident sequence. As reference plant Zaporozhye-5 was selected. The accident is initiated by a small break LOCA (80 mm diameter) in the hot leg followed by loss of offsite and onsite electric power (S<sub>1</sub>B-sequence). Recently performed PSA analyses for VVER-440 plants show that this sequence has a large contribution to core melt frequency [9, 10].

## 2. S<sub>1</sub>B-SEQUENCE

A particular accident scenario can be represented by an alphabetized sequence. In our case we consider a small break LOCA in the hot leg followed by loss of offsite and onsite electric power which is represented by S<sub>1</sub>B. S<sub>1</sub> stands for a small LOCA with an equivalent diameter of about 2-6 inches. B symbolizes failure of electric power.

Fig. 2 shows the most important accident phenomena during a severe accident. In a LOCA the primary system pressure drops rapidly till the saturation state is reached. When the saturation temperature is reached steam generation in the core starts. However water will still leak till the break level is reached. After some time core uncovering starts and the core heats up rapidly. Now the core starts to melt and finally it collapses into the bottom head.

Core slumping generates more steam and results in an increase of containment pressure. Some time later the reactor vessel is dry and due to the increasing temperatures the reactor vessel will fail. Now the discharge of the accumulators into the reactor cavity is initiated. The evaporation of the accumulator water leads to a rapid pressure rise.

The interaction between core debris and concrete generates a considerable amount of hot steam and gases resulting in a pressure increase and a rise of containment structure temperatures. The high structure temperatures cause a release of steam from the concrete. These effects lead to a pressure increase which can surmount the containment failure pressure causing a leak in the containment.



When melting of the core occurs the first fission products are released into the containment atmosphere. Due to the different transport mechanisms only a part of the fission products reaches the containment and the environment. Hydrogen and other non-condensable gases as CO and CO<sub>2</sub> are released by the core-concrete interaction. An important point is if the ignition point of hydrogen can be reached. In most cases the amount of generated steam is big enough to avoid an ignition of the hydrogen-air mixture.

Most of the released aerosols and fission products are deposited on surfaces within some hours. However each melting of the core adds more aerosols to the atmosphere. Therefore the time of containment failure is very important in the accident analysis. For instance in the case of Cs and I these elements will be deposited on structures after several hours and the largest fraction of the source term are the aerosols released during the core-concrete interaction.

### 3. INPUT-DATA

#### 3.1 MARCH3

One of the goals of this work was the improvement of the input-data base. In the first calculations for the TMLB'-sequence the input-data were based only on typical VVER-1000 features taken from the open literature [13]. In the meantime it was possible to collect MARCH3 data for the russian plant Zaporozhye-5 [14]. This plant was connected to the grid on Aug. 14, 1989 and therefore its data are topical.

Compared to the TMLB'-input set two kinds of changes were made:

- Changes to define the new sequence
- Changes to improve the reactor data according to the reference-plant.

Among the numerous data changes the most significant ones are mentioned below. Changes due to the first item are indicated by (S), changes due to the second item are indicated by (R).

To perform a MARCH calculation three different input-files are necessary: IN2, IN4 and IN5. IN2 contains the default values and IN4 stores the error messages. The largest amount of input data is on file IN5 which is organized in 12 namelist-groups.

IN5

NAMELIST NLMAR (Problem execution)

(S) IBRK = 1 indicates a small break  
(S) IECCXX = 0 no ECC considered  
(R) TOTAL the inventory is modified, big changes are  
in the following elements

Te (-50%)	Ag (-100%)
Sb (-50%)	Cd (-100%)
Sn (-99%)	In (-100%)
Tc (+50%)	Nb(+6600%)
Zr (-50%)	Pu (+25%)
Mn (-80%)	

NAMELIST NLSLAB (Containment wall heat sinks)

The containment wall is composed of two materials: concrete (set CONC1 = CONC2 = CONC3) and iron. The values for density, thermal conductivity and heat capacity are close to the standard values.

According to the containment geometry (see Fig. 3 and 4) the containment walls are divided into following slabs:

(R) ISLAB (I) = OUTCYL ... outer cylindrical wall  
DOOM ... top (dome) of containment  
FLOOR ... central floor at elevation 36,6 m  
PERECR ... outer floor at elevation 36,6 m  
INNERCYL.. inner cylindrical wall  
INCYLPG .. wall between pressure vessel and  
steam generators  
WALLPG1.. outer wall of steam generator room I  
WALLPG11. outer wall of steam generator room I  
WALLPG2.. outer wall of steam generator room I  
WALLPG22. outer wall of steam generator room I

FLCELSH.. floor of steam generator room  
FLCESH1.. floor of steam generator room  
CRAN .... )  
ST1 .... ) walls in the cran region  
ST2 .... )

- (R) NNO1 = number of nodes in the left material region  
= 3 for all slabs except the cran slabs (=5)
- (R) NNO2 = number of nodes in the right material region  
= 10 for all slabs except the cran slabs (=0)
- (R) SAREA = area of one face of slabs; the area varies at about one  
to several thousand m<sup>2</sup> according to the geometry.
- (R) TEMP = initial temperature of nodes; varies between 315 and  
391 K

NAMelist NLECC (ECC data)

- (R) P(N) = high pressure shutoff head for ECC pumps;  
values between 2.5 and 16.0 MPa are selected in  
contrary to the default value of 0.
- (R) PACMO = the initial accumulator pressure is slightly higher  
than before
- (R) PUHIO = initial pressure of upper head injection tank is  
selected to 5.9 MPa
- (R) RWSTM = 90 000 kg initial mass of water in the spray and ECC  
storage tank
- (R) TM = 30 and 40 sec ... start time for ECC pumps



NAMELIST NLBOIL (primary system models)

(S) ABRK = 0.00502 m<sup>2</sup> initial area of break for small  
LOCA

(R) ACOR = 4.17 m<sup>2</sup> core flow area

(R) AH heat transfer areas for the structures:

= 27,75 m <sup>2</sup>	- fint upper grid plate
284,5 m <sup>2</sup>	- guide tube
358,4 m <sup>2</sup>	- piping
6137 m <sup>2</sup>	- steam generator
99,33 m <sup>2</sup>	- grid plate
37,0 m <sup>2</sup>	- lower grid plate
26,87 m <sup>2</sup>	- bottom head

These values differ significantly from the values used in the TMLB'-case.

(R) ATOT = 7,37 m<sup>2</sup> total cross sectional area of water  
in vessel

(R) CLAD =  $7,3 \cdot 10^{-4}$  m effective clad thickness

(R) CM = mass times heat capacity of structures; values differ regarding to the different size of the structures

(R) FULSG = 198 785 kg mass of water in steam generator  
secondary

(R) NR = 50 856 total number of fuel rods in core

(R) PSG = 5.9 MPa steam generator secondary relief  
valve setpoint; it is 10% lower than in the  
TMLB'-case

(R) TAFW = 493 K temperature of steam generator secondary  
makeup water

- (R) TFAIL2 = TFAILB = TFAILX = 1672 K  
all failure temperatures are lowered to 1672 K
- (R) VOLPX = 370 m<sup>3</sup> total volume of water and steam  
within reactor coolant system primary pres-  
sure boundary
- (R) WATBHX = 14830 kg mass of water which could be  
stored in bottom head; this value is about  
30% lower than in the TMLB'-case
- (R) WBAR =  $9.3 \cdot 10^7$  J/K heat sink in BOIL and HEAD; the  
value is 10-times larger than in the TMLB'-  
case
- (R) WCST = 100 000 kg mass of water available for makeup  
to the steam generator secondary; the value  
is a factor of 500 lower than in the previous  
case

NAMELIST NLHEAD (bottom head heatup data)

- (R) DBH = 4.136 m diameter of hemispherical bottom head
- (R) THICK = 0.2 m thickness of bottom head
- (R) TMLTXX = 2373 K melting temperature of debris in  
bottom head

NAMELIST NLHOT (debris-water interaction data)

- (R) ACAV = 35,66 m<sup>2</sup> heat transfer area of top of debris  
bed in reactor cavity. This value is 20%  
lower than in the previous case.

NAMELIST NLCRCN (concrete-debris interaction data)

The concrete is composed of 10 different species:

(R) CNAME: Fe<sub>2</sub>O<sub>3</sub>  
          K<sub>2</sub>O  
          CdO  
          MgO  
          SiO<sub>2</sub>  
          Al<sub>2</sub>O<sub>3</sub>  
          MnO  
          CO<sub>2</sub>  
          H<sub>2</sub>O  
          Ca(OH)<sub>2</sub>

The mass fractions SM correspond to the new composition.

(R) HIT     = 8.59 m height of the cylinder of the  
            crucible  
HTWAL     = 3.05 m distance between debris and reactor  
            vessel  
RAD        = 3.25 m radius of the cylinder of the  
            crucible  
RW         = 5.25 m outside radius of crucible

3.2 TRAP-MELT3

To perform a TRAP-MELT calculation 4 input-files are  
necessary: IN1, IN5, IN10 and IN20

IN1

This file contains the geometry of the reactor and in-  
formation on the accident sequence.



The problem starts with core uncovering at 877 s and stops at start of hotdrop at 5961 s.

In the sequence the break occurs in the hot leg. To calculate fission product transport in such a case the primary system is divided into 4 volumes:

Core, upper plenum, hot leg and containment

The structures in these volumes are:

Core wall in the core;

Core plate, tubes & columns, support casting  
and core barrel in the upper plenum;

Hot leg wall in the hot leg;

Containment wall in the containment.

One of the input data for the core is the gas temperature, which is taken from MARCH-output OUT20 (TGEXC = 504.5 K). All the wall temperatures are set to this value except the containment wall temperature (375 K).

Due to lack of primary data for the primary system most of the necessary data are estimated values. Important tools for the estimation are the rate of volume and the rate of area between VVER-440 and VVER-1000 reactors. Basic values are taken from [15] and [16]. The necessary input data are summarized in the following table 1:

Both matrices for control volume flow connection and fraction of mass flow are kept as easy as in the sample problem.

Table 1:

TRAP-MELT3 input data (IN1)

Volume	Structure	Gas Volume VOL(ft <sup>3</sup> )	Length LL(ft)	Height HGT(ft)	Flow area AR1(ft <sup>2</sup> )	Mass x spec.heat CM(Btu/F)	Hydr.diam. DD(ft)	Length LL1(ft)	Wall Thickness DELX1(ft)	Surf.Area AH(ft <sup>2</sup> )	Settl.Area SETTL(ft <sup>2</sup> )	Fraction FBX(-)
Core	Core Wall	519.1	11.65	11.65	44.56	1.0	0.381	11.65	0.98	390.0	87.6	0.
Upper Plenum	Core Plate	1670.4	14.7	14.7	70.0	2226.0	0.0298	1.22	0.0104	507.0	4.57	0.5
	Tubes&Columns					1680.0	1.6	13.8	0.015	3450.0	0.	0.
	Support Casting					13545.0	5.0	15.5	0.2667	306.8	0.	0.
	Core Barrel					7222.0	0.105	8.8	0.118	857.0	0.	0.
Hot Leg	Hot Leg Wall	159.0	65.6	1.6	2.05	5821.0	1.60	65.6	0.1042	387.5	76.3	0.
Containment	Containment Wall	2472 000.0	1312.0	164.0	21 000.0	1.0	1.0	1.0	1.0	1.0	0.	0.

IN5

This unit contains the control parameters for fission product phenomena. Following mathematical parameters are chosen:

DIV = 20  
DTMIN = 1.  
MATSA = 0.01

In the first volume particle deposition and revaporization are allowed to occur, in the second volume vapor deposition, particle deposition and fall back. In the hot leg only vapor deposition and particle deposition are allowed. The geometric mean radius of the particle distribution is 0,05  $\mu\text{m}$ , the standard deviation is 1.7 and the mean particle density in all volumes is 3,0 g/cm<sup>3</sup>.

IN10

The contents of this file is the core inventory at start of accident and the course of fission product release from the core. This file is generated by MARCH3 (OUT10).

IN20

IN20 is a binary file containing the thermalhydraulic data for the core (Volume 1). This file is generated by MARCH (OUT20).

### 3.3 VANESA

Three input-files are necessary for a VANESA-calculation: IN3, IN4 and IN5.

#### IN3

In the first line of the file there is the title of the run, in the second line the time of the end of hotdrop (244.765 min) and the NAUA source mode (0 and 2) are indicated.

#### IN4

IN4 contains the main input for VANESA. The items are the core-inventory at start of accident and the course of release rates during the interaction. This file is generated by MARCH (OUT33).

#### IN5

The first line contains the title of the run, the second line the VANESA time-step (60,0 s), the third line is empty and the last one describes the 6 control variables for the subroutine POOL (-1 2.0 -1 -1 -1.0 -1.0).

### 3.4 NAUA and THCCA

NAUA needs information from six different sources. One file is compiled completely new (IN 5), others can be taken from different codes (IN2, IN11, IN14), and both IN12 and IN13 have to be changed before using them.

IN2

IN2 is a binary file which contains the volume of the preceding compartment and size, composition and flow rate of particles which leave the preceding compartment. This file is generated by TRAP-MELT3(OUT15).

IN5

This is the file for the control parameters. The first two lines contain the title, followed by a line with shape factors (1.0 1.0 1.0 0.01). Then there are data for particle classification. These data are the same as the corresponding data in TRAP-MELT3 (0.25E-6 5.0E-2 19 0.1 1.0E-30).

The next value for CPUZT represents the maximum CPU-time (2000.0). The following values stand for the number of leaks entering and leaving the compartment (1 1). The next 9 values are logical parameters to simulate the sequence (.F. .F. .F. .F. .T. .T. .T. .T. .T.).

Then the output time steps are necessary (200 1000 200) followed by the number of release periods for the particle source (34), the number of nuclides (11) and the number of title lines to be skipped (1). After the switch for steam condensation onto the walls (.T.) the times for the leak and size distribution tables are needed (10 3.0 3.5 4.0 5.0 6.0 8.0 10.0 12.0 14.0 16.0).

IN 11

This file contains the decontamination factors for each size bin as a function of time. It is generated either by SPARC (OUT08) or by ICEDF (OUT10). In our calculation it is not used.

IN 12

This file contains the "source"-information. It is composed of different parts. The final version has to be generated by hand.

After the title line there are the informations for the in-vessel release prior to vessel failure. The first value is the source rate (0.0), then the kind of release (.T.) indicates a continuous release and at last there are the mean geometric radius, its logarithmic variance and the particle density (8.38E-06 0.693 4.46). The values for mode 1 are now repeated for mode 2. The data are completed with the time at end of release (14685.90s) which corresponds with end of hotdrop. This data set is followed by the amounts of the nuclides for both modes.

The same structure, but without the title line, is used for the following release periods. The second release period occurs during ten minutes after end of hotdrop. The data are taken from the last part of the TRAP-MELT3 output OUT12. This information is completed by the release mass fractions of external particles (PE - from VANESA-output OUT08) and inert tracer (TR-1.47E-03).

The third release period on the input is identical with VANESA-output OUT08 except the title line. All these periods represent the complete ex-vessel-release.

IN13-THCCA

This file contains geometric and thermohydraulic data and the initial inventory. The main structure of the file is generated by the data reduction code THCCA (OUT03).

THCCA uses MARCH output-file OUT07 as an input-file (IN7) in addition to the file IN1. In IN1 the number of intervals and the size of the intervals are defined. The 45 intervals are chosen regarding the containment pressure response taken from the MARCH results. As a result of the use of THCCA the file OUT03 is generated.

The first text lines in THCCA.OUT03 are replaced by a line which contains VOLUME1. Then the noble gas inventories (NG) are deleted. In addition the inventories of the external particles (PE) and of the inert tracer (TR; 100 g) are necessary. Then the rest of THCCA.OUT03 can be taken. It contains for 44 grid points gas temperatures, net steam rate, steam condensation rate, leak rate, pressure and wall temperatures.

#### IN 14

IN 14 contains the same information as IN 2 but for a second leak. In our calculation this file is not used.

#### 4. RESULTS

##### 4.1 MARCH3 - Thermalhydraulics

BOIL. Subroutine BOIL calculates the thermalhydraulic response in the primary system during the accident. The most important events are summarized in the following Table 2:

Table 2: MARCH: S<sub>1</sub>B-Events

Time (s)	Event
877	Core uncover
1 404	Start of fission product release from fuel
2 024	Start of core melting
3 811	Core slumping
3 912	Start bottom head heatup
4 377	Vessel dryout
5 901	Bottom head failure
5 961	Start of hotdrop, accumulator discharge
10 786	Cavity dry
14 686	End of hotdrop
14 686	Start of core-concrete interaction
14 724	Containment failure due to overpressurization
18 226	Layer flip
50 686	End of core-concrete interaction

Fig. 5 illustrates the water inventory of the steam generator in the secondary side. In the first 800 s the water is evaporated to remove the decay heat of the primary system. When a water mass of 189 500 kg is reached the water inventory is kept constant.

The primary system pressure response is shown in Fig. 6. As a result of the break in the hot leg of the primary circuit the pressure drops rapidly in the first 50 seconds from the initial 15.7 MPa to 6.5 MPa. At this



pressure the temperature of the coolant is equal to the saturation temperature and steam generation in the core starts. This causes a slight increase of the pressure. The water is still leaking till the break level at 5.15 m is reached (566 s). For small LOCA's the MARCH-model assumes water leakage when the break is below the liquid level and gas leakage when the break is above the water level. This assumption has an effect on the discharge flow rate and therefore the pressure gradient changes. At 877 s core uncovering starts and from now on only a part of the energy is used for steam generation. Therefore the primary pressure decreases faster than before. The lower end of the core is reached by the water level at 1390 s and again there is a change in the pressure gradient. Due to the increasing core temperature the core starts to melt and finally core slumping occurs at 3811 s. Now the steam generating rate rises again causing an increase in primary pressure. Moderated by the cooling effect of the steam generator pressure rise is stopped and depressurization starts until bottom head failure is reached at 5901 s.

Fig. 7 shows the primary system water inventory and illustrates the phenomena sketched above. Water is leaking through the break till the break level is reached at 566 s. Then the rest of the water is boiling off till the vessel is completely dried out and bottom head failure occurs.

The course of steam-water mixture level in vessel is shown in Fig. 8. Here again the events at 566 s, 877 s and 1390 s govern the decrease of the mixture level.

The maximum and average core temperatures are shown in Fig. 9. After beginning of the accident the core is cooled down to the temperature of the coolant of about 550 K. Core uncovering at 877 s causes the rise of the core-temperatures up to the melting temperature of 2372 K. The average core temperature is increasing monotonously. After the disintegration of the core at 3811 s the geometry and the nodes are not defined and the line falls to zero.

In Fig. 10 the fraction of reacted cladding and the fraction of melted core (dashed line) is presented. The course of the plot is input-dependent. In this case meltdown model A is used which means that a molten region forms in the core and grows downward in such a manner that the average temperature of the region remains at the melting temperature. This model maximizes the downward movement of the molten pool. In addition there is a model for the metal-water reaction for the uncovered portion of the core. This model causes a fast increase of the material reacted. The slumping of the initial core nodes into the water in the vessel head produces large amounts of steam. This steam flows up and reacts with the high temperature cladding surfaces. The energy associated with the reactions leads to further core melting and finally to the collapse of the entire core into the vessel head. 93% of the cladding has been reacted and 65% of the core has been molten.

The behaviour of hydrogen which results from the zirconium-water reaction is illustrated in Fig. 11. (Dashed line is total amount, full line is amount in primary system). Hydrogen production starts at about 1300 s. Most of this gas is leaving the primary system through the leakage immediately, only a small amount is

retained in the primary system. Compared to the 500 kg hydrogen calculated in the TMLB'-calculation the amount of 62 kg is much lower.

The two curves in Fig. 12 show the temperatures of gases leaving the core (dashed line) and the temperatures of gases leaking to the containment (full line). The first mentioned temperatures can reach the maximum value of core temperature. The temperatures of the leaking gases however never exceed 1200 K. Due to the undefined core temperatures after 3811 s the gas temperatures show a distorted behaviour.

CORCON. The subroutine CORCON analyzes the concrete-melt interaction.

The initial interaction between the debris and the water in the sump keeps the debris in a quenched condition. Therefore the concrete-melt interaction starts with the heat-up of the debris.

Experimental evidence shows that the various oxidic species in the melt are highly miscible, as are the metallic species, but that the two groups are mutually immiscible. Practically the melt appears always in two phases: in an oxidic and in a metallic phase. The oxidic phase is initially denser than the metallic phase and settles to the bottom. A second less dense oxidic layer will form above the metal. It is composed of concrete oxides obliterated by the metal and steel oxides produced by chemical reaction with the concrete-decomposition gases.

The initial composition of the two layers is summarized in Table 3:

Table 3:

Oxide layer:	UO <sub>2</sub>	75 384	kg
	ZrO <sub>2</sub>	28 126	kg
	FPOX	1 428	kg
	FPALKMET	2,3	kg
	FPHALOGN	0,18	kg
	Fe <sub>3</sub> O <sub>4</sub>	803	kg
Metal layer:	Fe	20 382	kg
	Cr	5 241	kg
	Ni	2 912	kg
	Zr	1 581	kg
	FPM	376	kg

The initial temperature of the layers is 1728 K.

The heat flux to the concrete is sufficient to decompose it, releasing water vapor and carbon dioxide, and to melt the residual oxides. The surface of the concrete is obliterated at a rate which is typically several centimeters per hour. The molten oxides and molten steel from reinforcing bars in the concrete are added to the pool. The gases are strongly oxidizing at pool temperatures and will be reduced, primarily to hydrogen and carbon monoxide, on contact with metals in the pool. The reacted and unreacted gases enter the atmosphere above the pool.

Fig. 13 shows the radial (dashed curve) and the vertical (full line) progression of concrete attack. The interaction starts at 14 686 s (about 4 hours). After ten hours of interaction the depths of concrete attack are 87 cm and 119 cm. The initial thickness of concrete is 200 cm. After ten hours of interaction the thickness is decreased to 113 cm radially and to 81 cm axially.

The course of the melt cavity radius, which starts at 325 cm, is shown in Fig. 14. A picture of the concrete section with the progressing surfaces is presented in Fig. 15. The time interval between two surfaces is 6000 s. The initial concrete surface is at 8,59 m and the initial upper melt surface is at 8,06 m. Due to the interaction between melt and structural material the mass of the melt increases and therefore the melt surface rises up to 7,60 m (dashed-point curve). During the beginning of the interaction the melt progression is larger than in later times.

The sudden pressure increase due to the melt-concrete interaction is illustrated in Fig. 16. Fig. 17, Fig. 18 and Fig. 19 demonstrate the melt behaviour. The first picture shows the geometry of the pool. At first the metal layer is on the top, at 15 886 s a layer of light oxides starts to build up above the metal layer. At 18 225 s there is a layer flip and the metal layer is at the bottom from now on. Due to the continuing interaction between melt and structural material the mass of oxide is increasing generating an increasing oxide level. The second picture shows the average temperatures of the layers. At the beginning the temperatures of the layers rise. As time progresses the pool grows and its surface area increases. In addition the decay heat decreases. Therefore the pool temperatures and heat fluxes decrease and the possibility of refreezing arises (see Fig. 23 - 27). The corresponding interface temperatures are shown in Fig. 19. The effect of layer flip can be seen in Fig. 20 which shows the course of density of the different layers (1 = light oxide, 2 = metal, 3 = heavy oxide). There is a slight increase of density of the metal layer. Density of the heavy oxide layer is decreasing till it becomes equal to that of the metal. Now the

two oxide layers combine to form one, which is less dense than the metal.

In addition this behaviour can be seen in Fig. 21 which shows the course of mass of layers. Fig. 22 illustrates the increase of silica-content in the melt, Fig. 23 shows the layer void fraction and Fig. 24 represents the layer interface heat-flow.

When pool temperatures fall to the point where solidifications begins a crust will form. For the early stages there is the assumption of a crust at one or more interfaces around a remaining liquid. At later times considerable freezing may occur. If part or all of a layer becomes frozen, heat can be removed from it by conduction only, which is ordinarily far less effective than convection. Because of internal heating and the fact that cooling cannot continue unless heat losses exceed sources, freezing is largely self-limiting. Substantial freezing of the metallic layer may occur, but in the layer containing fuel oxides the volumetric heating is much greater and the thermal conductivity much lower so that only thin crusts can form.

In Fig. 25 - 27 the crust behaviour is illustrated. In combination with Fig. 17 it is possible to summarize the crust results:

At the beginning of the interaction there exist a 41 cm thick oxide layer in a solid state and a 13 cm thick metal layer in a liquid state surrounded by crusts. When the light-oxide layer appears as third layer it has the same condition as the heavy-oxide layer. At the end of the calculation there is at the top a 116 cm thick oxide layer in a liquid state without any crust. The 13 cm thick metal layer is in a solid state.

As mentioned above several gases are released during the decomposition of the concrete. Water vapor and carbon dioxide are reduced primarily to hydrogen and carbon monoxide. It is possible to further reduce carbon monoxide to atomic carbon. Fig. 28 - Fig. 30 shows the release behaviour of the most important gases. At the end of the calculation following amounts of gases are released (Table 4):

Table 4:

H <sub>2</sub> O	8 547	kg
H <sub>2</sub>	747	kg
CO <sub>2</sub>	51	kg
CO	30	kg
CH <sub>4</sub>	1	kg
H	0,025	kg
C <sub>2</sub> H <sub>2</sub>	0,012	kg

During the debris-concrete interaction the composition of the pool is changing continuously due to the varying physical and chemical conditions. Because we have three layers in the pool it is necessary to analyze the pool composition for each layer. The different fission products and actinides are grouped as four pseudo elements:

FpM	- metals which may oxidize and whose oxides may volatilize
FpOx	- chemically inert oxides
FpAlkMet	- alkali metals
FpHalogn	- halogens

FpM is included in the metal element list, the remaining three groups are included in the oxide element list.

The pool composition of the different layers during the debris-concrete interaction is shown in Fig. 31 - 37. The numbers of the curves correspond to the order of the element list in the title.

MACE. Subroutine MACE calculates the thermal-hydraulic behaviour of the containment.

The courses of pressure and temperature in the containment are illustrated in Fig. 38 and Fig. 39. In the first picture the full line represents the total pressure, the next line the steam pressure and the lowest one the hydrogen pressure. The line in between represents the sum of the pressures of the other gases. When the water is evaporating the pressure is increasing the first 877 s. At this time core uncovering lowers the boil-off rate. While the core is heating and beginning to melt the containment pressure decreases due to heat absorption by structures. Core collapse at 3811 s generates further steam and results in an increase of pressure. 460 s later the reactor vessel is dry and due to the increasing temperatures reactor vessel failure occurs at 5961 s. Now there is the discharge of the accumulators into the reactor cavity. The evaporation of the accumulator water leads to a rapid pressure rise at this time. This accumulator water in the reactor cavity evaporates till the reactor cavity is dry at 10 786 s.

Due to the reduced boiloff rate the containment pressure decreases faster.

At 14 686 s the debris-concrete interaction starts. The concrete surfaces are heated due to steam condensation (see Fig. 39) and release now a lot of steam according to the degassing model. This leads to a pressure spike



above the design level of the containment (0.8 MPa). In this calculation 490 000 kg steam are released during the first 630 seconds. Because of this high number it is recommended to check the degassing model in the STCP. The pressure spike generates containment failure. Now a leaking rate of 1 volume percent per day and a continuous pressure decrease is assumed. The total volume of gases leaked through the leakage is shown in Fig. 40.

The next Fig. 41 represents the corresponding temperatures of different containment structures. The range of the temperatures is between 315 and 445 K.

Fig. 42 illustrates the water inventories in the containment sump and in the reactor cavity (dashed line). At first the cavity is dry. The discharge of the accumulators leads at once to the evaporation of a part of the water due to the interaction between debris and core. The rest of the water is boiled off by the decay and stored heat. The containment sump water inventory increases as the steam released from the primary system condenses on the containment structures. An additional increase occurs at bottom head failure when the reactor cavity water starts to boil. The steep increase of water inventory after start of core-concrete interaction is due to the large amount of steam released from the concrete structures in the containment according to the degassing model. This steam condensates almost immediately on the walls and contributes to the sump water inventory. Fig. 43 shows the corresponding temperatures to these phenomena.

CORSOR. Subroutine CORSOR calculates the fission product release from the fuel in the core and from the molten debris during the in-vessel phase.

At 1390 s the lower end of the core is reached by the water level and fuel temperatures rise high enough to cause fuel rod failure and fission product release. This phenomenon starts at 1404 s. In the group of volatile fission product species there are the noble gases, iodine and cesium with very similar release rates at high temperatures. This similarity of their release is a result of similar transport processes in the fuel and their high volatilities. At time of core slumping already 88% of the inventory is released. Very similar is the situation for the Cs-compounds which are again released with 88%.

Tellurium has a slightly lower release rate but its release is complicated by interaction with Zr in the cladding. CORSOR contains an empirical model for this situation. In our case 75% of the inventory is released at time of core slumping.

From the low volatile species only small amounts are released and generally the release of them starts later, when fuel temperature reaches the melting point. At time of core slumping following amounts are released (Table 5):

Table 5:

Ba	0,3 %
Structural material	0,03%
Sr	0,01%
Ru	$1,0 \cdot 10^{-5}$ %
La	$3,0 \cdot 10^{-7}$ %

Details can be seen from the figures. Fig. 44 - 47 represent the amount of fission gas release of 24 different species according to the CORSOR-groups. The next four figures show the fraction of released inventory according to the CORSOR-groups (see Table 6).

For the rest of the calculation the species are summarized into ten groups (TRAP-group). The following Table 6 shows the relations between the CORSOR and the TRAP groups:

Table 6:

$$\begin{aligned} \text{CI} &= 260/127 * [\text{J} + \text{Br}] \\ \text{CH} &= 150/133 * [\text{Cs} + \text{Rb} - 133/260(\text{J} + \text{Br})] \\ \text{PI} &= \text{Ag}(\text{f}) + \text{Sn} + \text{UO}_2 + \text{Zr}(\text{st}) + \text{Fe} + \text{Cr} + \text{Ni} + \text{Mn}(\text{st}) + \\ &\quad + \text{AG}(\text{CR}) + \text{Cd}(\text{CR}) + \text{In}(\text{CR}) \end{aligned}$$

CR ... Control rod  
f ... Fission product  
st ... Structural

$$\begin{aligned} \text{TE} &= \text{Te} + \text{Sb} + \text{Se} \\ \text{SR} &= \text{Sr} \\ \text{RU} &= \text{Tc} + \text{Mo} + \text{Ru} + \text{Rh} + \text{Pd} \\ \text{LA} &= \text{Zr}(\text{f}) + \text{La} + \text{Nd} + \text{Eu} + \text{Nb} + \text{Pm} + \text{Pr} + \text{Sm} + \text{Y} \\ \text{NG} &= \text{Xe} + \text{Kr} \\ \text{CE} &= \text{Ce} + \text{Np} + \text{Pu} \\ \text{BA} &= \text{Ba} \end{aligned}$$

The amount of fission product release for the TRAP groups is shown in Fig. 52 - 54. The corresponding fractions of inventory are illustrated in Fig. 55 - 56.

After core slumping the debris is cooled by water and the debris temperature decreases. Therefore the release rate is much lower than before. After dryout of bottom head at 5900 s the temperature increases again causing a new release of fission products. The amounts of released species at time of bottom head failure are summarized in Table 7.

Table 7:

	Group Symbol	%	kg
Noble gases	NG	99,9	334
Br-J-compounds	CH	99,9	162
Structural material	PI	7 · 10 <sup>-2</sup>	78
Cs-J-compounds	CI	99,9	33,8
Tellurium	TE	85,0	20,6
Barium	BA	0,35	0,3
Strontium	SR	2,0 · 10 <sup>-2</sup>	1,0 · 10 <sup>-2</sup>
Ruthenium	RU	1,8 · 10 <sup>-5</sup>	8,0 · 10 <sup>-5</sup>
Lanthanum	LA	4,5 · 10 <sup>-7</sup>	3,8 · 10 <sup>-6</sup>

#### 4.2 TRAP-MELT3-Fission Product Transport in Primary System

TRAP-MELT3 starts the calculation with core uncover at 877 s. After bottom head failure at 5916 s the calculation is stopped. For the simulation of fission product transport in the primary system a more detailed thermo-hydraulic calculation is necessary which is performed in the subroutine MERGE. For this reason the primary system is divided into 4 volumes:

Volume 1    Core

Volume 2    Upper Plenum  
               with 4 structures: Core Plate  
                                   Tubes and Columns  
                                   Support Casting  
                                   Core Barrel

Volume 3 Hot Leg

Volume 4 Containment

MERGE. Subroutine MERGE analyzes the thermohydraulics of the primary system.

The thermohydraulics of the primary system can be divided into three phases:

1. From core uncovering to core slumping (877 s - 3811 s)
2. From core slumping to the end of evaporation of water in the bottom head (3811 s - 4377 s)
3. From end of evaporation of water in bottom head to bottom head failure (4377 s - 5961 s).

Some figures will illustrate this behaviour.

Fig. 57 - 59 show the gas temperatures of the core (Vol = 1) of upper plenum (Vol = 2) and of the hot leg (Vol = 3). At first there is an increase of the temperature due to the increasing core uncovering. At about 2000 s the core temperature reaches the melting temperature and is kept constant until disintegration of the core (see Fig. 9). The following figures 60 to 62 illustrate the rate of gas flow. It is reduced because the water level in the core is decreasing and therefore the steam-zirconium-reaction is diminished. In addition the total mass of gas is reduced in the volumes (Fig. 63 for upper plenum and Fig. 64 for the hot leg). About 1400 s the cladding starts to react with steam (see Fig. 10) which causes a spike for hydrogen mass in the first period (Fig. 65 for upper plenum and Fig. 66 for the hot leg). The steam masses (Fig. 67 and 68) are almost identical to the total masses. Fig. 69 and 70 show the heat transfer rate in upper plenum and in hot leg. Because of the high temperatures of gases the heat is transferred from the gas to the structures.

In the second period the molten core falls into the water filled bottom head and a large amount of steam is produced (see spike in Fig. 60 to Fig. 62). Now the hot debris evaporates the water in the bottom head generating a high rate of gas flow. During this period the gas temperature drops to almost saturation temperature (Fig. 57 to Fig. 59) and hydrogen generation stops (see Fig. 65 and 66).

The third phase starts with vessel dryout at 4377 s. Now the rate of gas flow is decreased significantly and the temperatures start to rise again.

TRAP. This subroutine analyzes the fission product behaviour in the primary system. The results of the calculation are presented for 9 radionuclide groups and 4 geometrical volumes. The groups are CI, CH, PI, TE, SR, RU, LA, NG, BA according to Table 6. The volumes are core, upper plenum, hot leg and containment. The distributions of the radionuclides as functions of their physical and chemical status are illustrated in Fig. 71 - 106.

The radionuclide can exist as

- (1) suspended as vapor
- (2) suspended as particles
- (3) condensed on surfaces
- (4) deposited as aerosol
- (5) chemically reacted with surfaces.

In addition the sum of these curves is presented in Fig. 71 - 106.

In the case of CI the behaviour in the core is shown in Fig. 71. At the beginning of core melting the fission product release increases, mainly in the form of vapor.

After reaching a maximum value the release decreases to a minimum at time of core slumping. In the period up to vessel dryout the release as particles is dominating. After this period the material is heated again and the release rises again. Fig. 72 shows the behaviour in the upper plenum. Due to the large structure area much more material is in this volume. Most of CI is condensed on surfaces. A quite similar behaviour is shown in the hot leg (Fig. 73). Finally Fig. 74 illustrates the release into the containment which starts with core melting. The main form of CI is vapor. When particle release starts at time of vessel dryout this component is added to the vapor release. 28 kg from the initial 34,2 kg are released into the containment which corresponds to 82%. From the 5,8 kg material in the primary system 5,4 kg are deposited on surfaces which corresponds to 16% of the initial amount of CI.

Almost the same qualitative behaviour is shown for CH in Fig. 75 - 78. 135,6 kg are released into the containment which corresponds to 83%.

A different behaviour for the structural material PI is shown in Fig. 79 - 82. There is a low increase of PI release suspended as particles in the core volume up to start of melting through bottom head at 3900 s. When temperature is high again after 5000 s the release starts to rise again. From the initial 1058000 kg only 58,8 kg are released into the containment (0,0056%). However this amount is 75% of the CORSOR-release. From the 19 kg material in the primary system 16,5 kg are deposited on surfaces (87%).

Fig. 83 - 86 illustrate the TE behaviour. From the initial 24,4 kg (CORSOR 20,6 kg) only 7 kg are released into the containment. Most of the material has reacted chemically with surfaces mainly in the upper plenum and in the hot leg. TE released into containment is mainly suspended as vapor.

SR behaviour (Fig. 87 - 90) is similar to PI behaviour. However only 7 g from the initial 49,6 kg (CORSOR 10 g) are released to the containment. Most of the material is released before core slump in form of particles. In the upper plenum and in the hot leg most of SR is deposited as aerosol leaving 2,2 g in primary system.

The RU-results (Fig. 91 - 94) are not significant because of the low amounts of material. From the 0,08 g released from the fuel only 0,06 g pass into the containment.

The same behaviour is shown for LA (Fig. 95 - 98). From very small release ( $4,5 \cdot 10^{-7}\%$  of core inventory) 73% of the material passes into the containment (0,03 g). Most of the material in the upper plenum and in the hot leg is deposited as aerosol. The 334 kg noble gases are passed almost entirely into the containment (331,5 kg, see Fig. 99 - 102).

The last four figures (Fig. 103 - 106) show the behaviour of BA. 0,223 kg are released into the containment which corresponds to 0,34% of the inventory. BA is suspended as particles in the containment, deposited as aerosol in the upper plenum and in the hot leg.

The most important results are combined in 3-D plots (Fig. 107 - 115). The progression of mass in time and system is shown. The units of the time-axis are seconds, the units of the mass axis are grams. The upper plot



illustrates the mass deposited in primary system, the plot in the center shows the mass suspended in primary system and the lower plot presents the sum of the upper values.

Summarizing the results it is shown that

- 99% of the noble gases
- 34% of tellurium
- 70 - 84% of the other elements

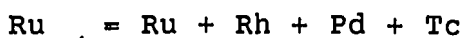
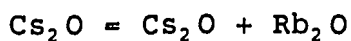
are released to the containment.

#### 4.3 VANESA - Fission Product Release during Debris-Concrete Interaction

Chapters 4.1 - 4.2 describe the in-vessel behaviour of the fission products and aerosols. However due to the debris-concrete interaction radionuclides can be generated outside the vessel. This phenomenon is simulated with the code VANESA.

The calculation starts with the beginning of the core-concrete interaction at 14 686 s and stops 10 h later at 50 686 s.

The main influence on fission product behaviour comes from the melt composition and from the gas flow through the melt. Some of the elements in the melt are summarized in groups of similar chemical behaviour. These groups are indicated by following symbols:



In chapter 4.1 the initial mass of non-fission elements are presented (Table 3). Now there is the list of initial mass of fission products.

Table 8:

Fission product	initial mass (kg)
CeO <sub>2</sub>	715
La <sub>2</sub> O <sub>3</sub>	511
Nb <sub>2</sub> O <sub>5</sub>	323
Ru	254
Mo	171
Ba	72
Sr	59
Te	4.7
Ag	2.4
Cs <sub>2</sub> O	2.0
Sb	0.5
CsJ	0.4

All these masses are calculated in MARCH.

In VANESA there are two models for aerosol production [17]:

1. Vaporization
2. Mechanical production.

Vaporization is the most important of the mechanisms leading to release of radionuclides and generation of aerosols during core debris interaction with concrete.

Vaporization occurs mainly when core debris temperatures are highest. This phenomenon is the reason that aerosols can be enriched in debris constituents relative to the condensed phase core debris. Analysis of vaporization involves both thermodynamic and kinetic considerations. These consideration must be taken separately for the oxide and metallic phases. The thermodynamic analysis establish the driving force and the maximum extent of vaporization of core debris constituents. The kinetic analyses determine the approach to the maximum extent of vaporization of core debris.

The mechanical model of aerosol production is based on the fact that gases move in form of discrete bubbles through the melt. At the surface of the molten core debris the bubbles burst. The burst of bubbles is known to create some of the highest material accelerations obtained on earth. This leads to melt material being thrown upward in very small droplets which contribute to the aerosol mass. However at higher gas velocities the droplets will grow and fall back into the melt pool.

In our calculation it is shown (Fig. 116) that most of the aerosols are generated in the first 5000 s due to the high initial temperature (Fig. 117). However no aerosols are generated mechanically. The aerosol density is illustrated in Fig. 118. In addition the temperature dependent process determines the aerosol particle size which is one order of magnitude higher in the vaporization phase (Fig. 119).

A similar behaviour is illustrated for the total mass of aerosols in Fig. 120. The composition of aerosols released from the debris is shown in Fig. 121 - 125. Here again the concrete constituents play a dominant role in the first 5000 s. At time 23 000 s  $K_2O$  is the main constituent followed by  $UO_2$  and Te.

Fig. 126 and Fig. 127 demonstrate the mole composition of gases leaving the debris and the gas generation rate. The zirconium reaction produces at first hydrogen as main gas. At 23 000 s steam production increases up to 32%. The other gas do not contribute to the gas composition. Finally we obtain following contribution: 67% H<sub>2</sub>, 32% H<sub>2</sub>O, 0,2% CO and 0,03% CO<sub>2</sub>.

The following Table 9 summarizes the masses of elements which are released during 10 hours of debris-concrete interaction:

Table 9:

<u>Fission products</u>	Mass [kg]	Release fraction
J+Br	0,2	1,0
Cs+Rb	1,9	1,0
Te+Se	1,4	0,43
Sb	7,3.10 <sup>-4</sup>	1,3.10 <sup>-3</sup>
Sr	2,5	5,1.10 <sup>-2</sup>
Mo	4,1.10 <sup>-3</sup>	2,4.10 <sup>-5</sup>
Ru+Tc+Rh+Pd	9,5.10 <sup>-5</sup>	3,7.10 <sup>-7</sup>
La+Y+Zr	2,0	3,6.10 <sup>-3</sup>
Nb	20,9	9,2.10 <sup>-2</sup>
Ce+Np+Pu	3,3	3,7.10 <sup>-3</sup>
Ba	1,9	2,9.10 <sup>-2</sup>
<u>Core material</u>		
Fe	15,8	2,1.10 <sup>-4</sup>
Cr	1,8	3,3.10 <sup>-4</sup>
Ni	13,1	4,5.10 <sup>-3</sup>
Mn	1,2	0,26
Zr	0,16	7,3.10 <sup>-6</sup>
Sn	3,3.10 <sup>-3</sup>	4,3.10 <sup>-2</sup>
Ag	0,37	0,15
U	8,5	1,3.10 <sup>-4</sup>
<u>Concrete</u>		
CaO	8,20	3,1.10 <sup>-4</sup>
Al <sub>2</sub> O <sub>3</sub>	2,7	2,7.10 <sup>-4</sup>
Na <sub>2</sub> O	0	0
K <sub>2</sub> O	28,2	0,11
SiO <sub>2</sub>	43,3	3,5.10 <sup>-4</sup>

#### 4.4 NAUA - Fission Product Transport in Containment

The calculation of fission product transport in containment is performed by the code NAUA [18]. It is based on mechanistic modelling of aerosol agglomeration and depositions within a containment vessel where there may exist a condensing steam atmosphere.

NAUA calculates only physical processes but no chemical reactions or radioactive decay is considered. Following assumptions are made:

- Particles are homogeneously distributed in a control volume except for the boundary layers at the walls.
- Within one particle size class no difference in particle composition is allowed.
- Particle properties are functions of only one independent variable, the particle size, and of the particle density which may change, due to varying particle composition.
- Process coefficient (shape factors, boundary layers etc.) are assumed to be independent on particle size.

For melt accidents these assumptions are considered to be valid. In a control volume the code calculates the following processes:

- Removal processes: Gravitational settling  
Diffusional plate out  
Diffusiophoresis
- Particle growth processes:  
Brownian coagulation  
Gravitational coagulation  
Steam condensation on particles
- Transport processes:  
Aerosol sources  
Leakages
- Engineered safety features:  
Spraying  
Suppression pool  
Ice condenser

In our accident sequence there is only one containment and no operating safety features. Therefore only one NAUA run is necessary to model containment fission product transport. The geometric and thermal hydraulic data come from MARCH, the fission product source information comes from TRAP-MELT3 and VANESA.

At a time prior to core uncover (867 s) the steam concentration is calculated by MARCH and passed to NAUA. The run start was chosen to 1395 s when fission product release from fuel begins. 34 releases during accident time are assumed.

Fig. 128 shows the particle number concentration in containment. After start of fission product release the concentration is growing up to 2000 s. Now the concentration decreases due to two effects. First there is a reduced flow to the containment because steam-zirconium reaction is diminished, and second the removal mechanisms in the containment become effective. At core slump (3811 s) the large amount of produced steam generates a new increase of particle number concentration. At 4377 s vessel dryout occurs and the gas flow rate is decreased again causing a dominant behaviour of the removal mechanisms. The start of the debris-concrete interaction at 14 686 s produces a lot of new particles. Caused by the layer flip in the melt at 18 226 s the layer temperatures decrease (see Fig. 18) reducing the particle generation rate (see Fig. 28). This effect in combination with the constant leakage of the containment generates an almost constant value for the particle number concentration.

Basically a similar behaviour of the total mass concentration is shown in Fig. 129. In the next figure 130 the different classes of particles characterized by the average radius illustrate the processes described above. In addition Fig. 131 shows the particle size distribution.

A more detailed behaviour can be studied in the following figures. All the physical processes mentioned at the beginning of this chapter are dependent on the size and the weight of the particles. Therefore it is necessary to specify the solid part and the liquid part of a particle. Fig. 132 illustrates the solid part of mass concentration. A comparison with Fig. 129 shows that there is no liquid component in the total mass concentration.

The main removal mechanisms are gravitational settling and diffusional deposition. The second process is caused by the gradient of the particle concentration in the laminar boundary layer which forces the particles to move to the surfaces where they are kept by Van-der-Waals forces. Fig. 133 shows the accumulated deposition due to gravitation. The following two figures 134 and 135 illustrate the solid and the liquid component. The containment atmosphere is completely dry except at time of bottom head failure. During several seconds some thousands kg of water are suspended in the containment generating the liquid part in Fig. 135. The liquid component is a factor of 20 lower than the solid part and vanishes immediately when the water is vaporized.

Fig. 136 shows the accumulated deposition due to diffusion. This mechanism removes four times more particles than gravitational settling. (The floor area of the containment is only one third of the total surface area). Fig. 137 and Fig. 138 represent the solid and the liquid part of the diffusional deposition. In this case the liquid component is a factor of 40 lower than the solid part.

Combining all these results the final figures are obtained. Fig. 139 shows the total airborne and the accumulated leaked masses. The initial sharp increase in the airborne mass indicates the in-vessel aerosol generation upon core melting and the aerosol release into the containment. The first maximum demonstrates that the removal mechanisms in the containment become effective from the beginning. The second maximum indicates start of debris-concrete interaction. The next Fig. 140 represents the accumulated leaked masses for each nuclide-group. Fig. 141 summarizes the fractions of leaked inventory for each group. The final numerical values are given in the following Table 10.

In this table for each nuclide-group the integral releases at the different computation steps are given. The sum of in-vessel release (TRAP-MELT3) and ex-vessel release (VANESA) is equal the sum of removed masses (NAUA removal) and airborne masses (NAUA airborne mass) in the containment. The last column shows the released fraction of inventory.



Table 10

Fractions of leaked inventory

Group	Initial Core Inventory [g]	CORSOR Release [g]	TRAP-MELT3 Release [g]	VANESA Release [g]	NAUA Removal [g]	NAUA Airborne Mass [g]	NAUA Release to environment [g]	Released Fraction of Inventory
NG	$3,36 \cdot 10^5$	$3,32 \cdot 10^5$	$3,31 \cdot 10^5$	0	0	$3,31 \cdot 10^5$	$1,55 \cdot 10^3$	$4,6 \cdot 10^{-3}$
TE	$2,44 \cdot 10^4$	$2,06 \cdot 10^4$	$7,06 \cdot 10^3$	$1,40 \cdot 10^3$	$8,31 \cdot 10^3$	$1,58 \cdot 10^2$	$1,43 \cdot 10^0$	$5,9 \cdot 10^{-5}$
CI	$3,42 \cdot 10^4$	$3,37 \cdot 10^4$	$2,79 \cdot 10^4$	$8,40 \cdot 10^2$	$2,87 \cdot 10^4$	$2,33 \cdot 10^1$	$1,43 \cdot 10^0$	$4,2 \cdot 10^{-5}$
CH	$1,63 \cdot 10^5$	$1,61 \cdot 10^5$	$1,35 \cdot 10^5$	$4,21 \cdot 10^3$	$1,39 \cdot 10^5$	$9,50 \cdot 10^1$	$6,46 \cdot 10^0$	$4,0 \cdot 10^{-5}$
SR	$4,96 \cdot 10^4$	$9,18 \cdot 10^0$	$6,94 \cdot 10^0$	$2,55 \cdot 10^3$	$2,50 \cdot 10^3$	$5,39 \cdot 10^1$	$1,86 \cdot 10^0$	$3,8 \cdot 10^{-5}$
LA	$7,97 \cdot 10^5$	$3,85 \cdot 10^{-3}$	$2,90 \cdot 10^{-3}$	$1,73 \cdot 10^4$	$1,69 \cdot 10^4$	$4,91 \cdot 10^2$	$1,70 \cdot 10^1$	$2,1 \cdot 10^{-5}$
BA	$6,54 \cdot 10^4$	$2,95 \cdot 10^2$	$2,24 \cdot 10^2$	$1,90 \cdot 10^3$	$2,05 \cdot 10^3$	$6,76 \cdot 10^1$	$1,42 \cdot 10^0$	$2,1 \cdot 10^{-5}$
CE	$8,95 \cdot 10^5$	0	0	$3,34 \cdot 10^3$	$3,27 \cdot 10^3$	$7,11 \cdot 10^1$	$2,46 \cdot 10^0$	$2,7 \cdot 10^{-6}$
PI	$1,06 \cdot 10^8$	$7,80 \cdot 10^4$	$5,88 \cdot 10^4$	$2,50 \cdot 10^3$	$6,13 \cdot 10^4$	$3,79 \cdot 10^1$	$2,66 \cdot 10^0$	$2,5 \cdot 10^{-8}$
RU	$4,26 \cdot 10^5$	$8,20 \cdot 10^{-2}$	$6,81 \cdot 10^{-2}$	$4,21 \cdot 10^0$	$3,39 \cdot 10^0$	$8,83 \cdot 10^{-1}$	$3,66 \cdot 10^{-3}$	$8,6 \cdot 10^{-9}$

## 5. DISCUSSION

In this specific small LOCA sequence the main events for the source term are start of fission product release at 1404 s, bottom head failure at 5901 s, start of core-concrete interaction at 14 686 s followed by containment failure at 14 724 s.

The fission products can be grouped into ten typical groups. The behaviour of these groups during the accident is calculated. It is possible to distinguish three classes of fission product groups:

- 1) Noblegases (NG)
- 2) Volatile gases (TE, CI, CH)
- 3) Low volatile gases (SR, LA, BA, CE, PI, RU)

The noblegases are released almost completely to the containment (fraction = 0,98). From here they are released to the environment with the assumption of a leakage of 1 volume percent per day. The calculation stops after 14 hours and in the discussion these final values are considered. In the case of the noblegases only a fraction of  $4,6 \cdot 10^{-3}$  of the initial inventory is leaked.

Tellurium exists mainly in elemental form (Te, Te<sub>2</sub>). A fraction of 0,85 is released from the fuel but most of it reacts chemically in the primary system. Only 0,29 is released to the containment. Finally  $5,9 \cdot 10^{-5}$  of the initial inventory leaks to the environment.

Cs and I react to CsI which is highly soluble in water. However there is not much water in the primary system to remove CsI. So a fraction of 0,80 reaches the containment. In containment all of this component of CsI is

removed in addition with a part of the ex-vessel generated component. Finally the released fraction is  $4,2 \cdot 10^{-5}$ .

In the steam/hydrogen atmosphere Cs exists mainly as hydroxide (CsOH). Its qualitative behaviour is very similar to that of CI resulting in almost the same release fraction of  $4,0 \cdot 10^{-5}$ .

The first fission product of the low volatile class in the discussion is SR. A big source is coming from ex-vessel generation. Most of the SR-material is kept in the containment and only a fraction of  $3,8 \cdot 10^{-5}$  is released to the environment.

As in the case before the main source of LA is coming from ex-vessel generation. Most of LA is removed in the containment.  $2,1 \cdot 10^{-5}$  of the initial inventory is released to the environment.

BA has the same number as release fraction however the processes are different. Much less BA is removed in the primary system. Contrary more BA is kept in the containment.

No CE release from the fuel is assumed and the only source comes from ex-vessel generation. With the same NAUA removal rate as for BA a release fraction of  $2,7 \cdot 10^{-6}$  is obtained. From the structural material (PI) only a fraction of  $7,3 \cdot 10^{-4}$  is released to the primary system. Here the removal rate is very small and 75% of the material is released to the containment. A second source is the ex-vessel generation. However a very strong removal rate in the containment results in a release fraction of  $2,5 \cdot 10^{-8}$ .

The main source for RU is ex-vessel generation, however most of the material is kept in the containment. Only  $8,6 \cdot 10^{-9}$  of the initial inventory is released to the environment.

All these numbers demonstrate that only very small fractions of the inventory leave the containment.

Compared with the TMLB'-results [8] much lower values are obtained. The total airborne and accumulated leaked masses are lower by a factor of 10. In addition most of masses for the specific groups are lower by a factor of 10. The main reason for this difference is the different initial inventory (see chapter 3.1). To make conclusions from a comparison between the results of the TMLB'- and the S<sub>1</sub>B-sequence a new calculation with the same inventory is necessary.

At last it should be stressed that the influence of some models - especially the degassing model - should be investigated because it determines the time of containment failure. A different time of containment failure can result in quite different release rates to the environment. In addition it must be mentioned that all results are based on the assumption of a containment leakage rate of 1 volume percent per day.

6. REFERENCES

- [1] USNRC, Technical Bases for Estimating Fission Product Behaviour During LWR Accidents, NUREG-0772, June 1981
- [2] W.F. Pasedag, R.M. Blond and M.W. Jankowski, Regulatory Impact of Nuclear Reactor Accident Source Term Assumptions, USNRC Report NUREG-0771, For Comment, June 1981
- [3] R. Blond et al., The Development of Severe Reactor Accident Source Terms: 1957-1981, USNRC Report NUREG-0773, November 1982
- [4] M. Silberberg et al., Reassessment of the Technical Bases for Estimating Source Terms, Final Report, NUREG-0956, July 1986
- [5] J.A. Gieseke et al., Source Term Code Package, A User's Guide (Mod 1), NUREG/CR-4587, BMI-2138, July 1986
- [6] USNRC, Reactor Risk Reference Document, Main Report, NUREG-1150, Febr. 1987
- [7] G. Sdouz, Implementierung des "Source Term Code Package" an der CYBER 180-860, ÖFZS-4496, EA-332/89 (März 1989)
- [8] G. Sdouz, Berechnung des Quellterms für einen TMLB'-Störfall bei einem Reaktor vom Typ WWER-1000, ÖFZS-4503, EA-335/89 (Juli 1989)
- [9] J. Misak, V. Polak, Z. Bazso, Cooling System Failures leading to Severe Accidents in WWER-440-Reactors following Small Break LOCAs, IAEA-SM-296/109, Symp. on Severe Accidents in Nuclear Power Plants, Sorrento, 21-25 March 1988

- [10] M. Kulig, J. Szczurek, Thermohydraulic Analysis for Supporting PSA of SB LOCA in WWER-440, IAEA-TC-560.03, p. 113, Computer Aided Safety Analysis 1989, IAEA Workshop, Berlin 17-21 April 1989
- [11] Proceedings of the International Seminar on Fission Product Transport Processes in Reactor Accidents, May 22-26, 1989, Dubrovnik
- [12] B. Kujal, J. Dienstbier, Severe Accident Analysis in Nuclear Research Institute, Computer Aided Safety Analysis 1990, IAEA-Workshop, Moscow, 14-17 May 1990
- [13] P. Nathschläger, Aufbau eines MARCH-3 Eingabedatensatzes für eine Anlage vom Typ WWER-1000 zur Initialisierung einer Quelltermstudie mit dem "Source Term Code Package", ÖFZS-4495, EA-331/89 (Februar 1989)
- [14] A. Shubenkov: personal communication
- [15] The STCP Application for the VVER-440-Reactors - Interim Report (1987-1988), IAEA-TCAC-RER/9/004
- [16] Overall Plan Design Descriptions: VVER Water-Cooled, Water-Moderated Energy Reactor: Revision 1 DOE/NE-0084-Rev. 1 (October 1987)
- [17] D.A. Powers, J.E. Brockmann, A.W. Shiver, VANESA: A Mechanistic Model of Radionuclide Release and Aerosol Generation During Core Debris Interactions With Concrete, NUREG/CR-4308, SAND 85-1370 (July 1986)
- [18] H. Bunz, M. Koyro, W. Schöck, NAUA Mod 4 - A Code for Calculating Aerosol Behaviour in LWR Core Melt Accidents; Code Description and Users Manual, KfK 3554 (August 1983)

7. LIST OF FIGURES

- 1 Structure of STCP
- 2 PWR Severe Reactor Accident Phenomena  
(from H.J. Teague et al: "A Generic Overview of Severe Accident Phenomena" in [11])
- 3 Elevation view of VVER-1000 reactor building (from [12])
- 4 Plan view of VVER-1000 reactor building (from [12])
- 5 Steam generator secondary side water inventory
- 6 Primary system pressure response
- 7 Primary system water inventory
- 8 Steam-water mixture level in vessel
- 9 Maximum and average core temperatures
- 10 Fraction of cladding reacted and fraction of core melted
- 11 Hydrogen produced and retained in primary system
- 12 Temperatures of gases leaving the core and leaked to the containment
- 13 Progression of concrete attack
- 14 Melt cavity radius
- 15 Melt progression in concrete  
(surfaces each 6000 seconds)
- 16 Ambient pressure above pool
- 17 Geometry of the melt
- 18 Temperature of the layers
- 19 Interface temperatures
- 20 Density of layers
- 21 Mass of layers
- 22 Mass of silica in melt

- 23 Layer void fraction
- 24 Layer interface heat flow
- 25 Top crust thickness
- 26 Bottom crust thickness
- 27 Side crust thickness
- 28 Cumulative release of gases from concrete
- 29 Cumulative release of gases from concrete
- 30 Cumulative release of gases from concrete
- 31 Pool composition of light oxide layer
- 32 Pool composition of light oxide layer
- 33 Pool composition of light oxide layer
- 34 Pool composition of metal layer
- 35 Pool composition of heavy oxide layer
- 36 Pool composition of heavy oxide layer
- 37 Pool composition of heavy oxide layer
- 38 Containment pressure response
- 39 Containment temperature response
- 40 Total volume of gases leaked from the containment
- 41 Containment structure surface temperatures
- 42 Containment sump and reactor cavity water inventories
- 43 Containment sump and reactor cavity water temperatures
- 44 Fission product release from the fuel (kg)  
- CORSOR group
- 45 Fission product release from the fuel (kg)  
- CORSOR group
- 46 Fission product release from the fuel (kg)  
- CORSOR group
- 47 Fission product release from the fuel (kg)  
- CORSOR group



- 48 Fraction of released inventory from the fuel (%)  
- CORSOR group
- 49 Fraction of released inventory from the fuel (%)  
- CORSOR group
- 50 Fraction of released inventory from the fuel (%)  
- CORSOR group
- 51 Fraction of released inventory from the fuel (%)  
- CORSOR group
- 52 Fission product release from the fuel (kg)  
- TRAP group
- 53 Fission product release from the fuel (kg)  
- TRAP group
- 54 Fission product release from the fuel (kg)  
- TRAP group
- 55 Fraction of released inventory from the fuel (%)  
- TRAP group
- 56 Fraction of released inventory from the fuel (%)  
- TRAP group
- 57 Core gas temperature
- 58 Upper plenum gas temperature
- 59 Hot leg gas temperature
- 60 Rate of gas flow in core
- 61 Rate of gas flow in upper plenum
- 62 Rate of gas flow in hot leg
- 63 Total mass of gas in upper plenum
- 64 Total mass of gas in hot leg
- 65 Hydrogen mass in upper plenum
- 66 Hydrogen mass in hot leg
- 67 Steam mass in upper plenum
- 68 Steam mass in hot leg
- 69 Heat transfer rate in upper plenum
- 70 Heat transfer rate in hot leg

- 71 Distribution of CI in core
- 72 Distribution of CI in upper plenum
- 73 Distribution of CI in hot leg
- 74 Distribution of CI in containment
- 75 Distribution of CH in core
- 76 Distribution of CH in upper plenum
- 77 Distribution of CH in hot leg
- 78 Distribution of CH in containment
- 79 Distribution of PI in core
- 80 Distribution of PI in upper plenum
- 81 Distribution of PI in hot leg
- 82 Distribution of PI in containment
- 83 Distribution of TE in core
- 84 Distribution of TE in upper plenum
- 85 Distribution of TE in hot leg
- 86 Distribution of TE in containment
- 87 Distribution of SR in core
- 88 Distribution of SR in upper plenum
- 89 Distribution of SR in hot leg
- 90 Distribution of SR in containment
- 91 Distribution of RU in core
- 92 Distribution of RU in upper plenum
- 93 Distribution of RU in hot leg
- 94 Distribution of RU in containment
- 95 Distribution of LA in core
- 96 Distribution of LA in upper plenum
- 97 Distribution of LA in hot leg
- 98 Distribution of LA in containment

- 99 Distribution of NG in core
- 100 Distribution of NG in upper plenum
- 101 Distribution of NG in hot leg
- 102 Distribution of NG in containment
- 103 Distribution of BA in core
- 104 Distribution of BA in upper plenum
- 105 Distribution of BA in hot leg
- 106 Distribution of BA in containment
- 107 Mass behaviour of CI
- 108 Mass behaviour of CH
- 109 Mass behaviour of PI
- 110 Mass behaviour of TE
- 111 Mass behaviour of SR
- 112 Mass behaviour of RU
- 113 Mass behaviour of LA
- 114 Mass behaviour of NG
- 115 Mass behaviour of BA
- 116 Created aerosols
- 117 Oxide melt temperature
- 118 Aerosol density
- 119 Mean aerosol particle size
- 120 Total mass of aerosol
- 121 Weight percent of released species
- 122 Weight percent of released species
- 123 Weight percent of released species
- 124 Weight percent of released species
- 125 Weight percent of released species

- 126 Mole percent of gases
- 127 Gas generation rate
- 128 Particle number concentration in containment
- 129 Total mass concentration in containment
- 130 Average particle radius
- 131 Particle size distribution
- 132 Solid part of mass concentration
- 133 Accumulated deposition due to sedimentation
- 134 Solid part of accumulated deposition due to sedimentation
- 135 Liquid part of accumulated deposition due to sedimentation
- 136 Accumulated deposition due to diffusion
- 137 Solid part of accumulated deposition due to diffusion
- 138 Liquid part of accumulated deposition due to diffusion
- 139 Total airborne and accumulated leaked masses in containment
- 140 Accumulated leaked masses
- 141 Fraction of inventory leaked

ÖEFZS-Berichte

Herausgeber, Verleger, Redaktion und Hersteller:

Österreichisches Forschungszentrum Seibersdorf Ges.m.b.H.

A-2444 Seibersdorf, Tel. (02254) 80, Telex 014-353

Alle Rechte vorbehalten.